PHYSICAL REVIEW B

CONDENSED MATTER

THIRD SERIES, VOLUME 49, NUMBER 11 15 MARCH 1994-I

Electron transport properties in RuO_2 rutile

Keith M. Glassford and James R. Chelikowsky

Department of Chemical Engineering and Materials Science, and Minnesota Supercomputer Institute, University of Minnesota, Minneapolis, Minnesota 55455

(Received 23 August 1993)

First-principles electronic-structure calculations were used to determine the electron-transport properties of RuO_2 in the rutile structure. Our calculations were performed within the local-density approximation employing soft-core *ab initio* pseudopotentials and a plane-wave basis. The two independent components of the tetragonal plasma-frequency tensor, $\Omega_{p,xx}$, and $\Omega_{p,zz}$, were found to be identical within the calculational errors. The calculated isotropy of the plasma-frequency tensor agrees with optical and transport measurements. Our theoretical value for the plasma frequency of 3.3 eV is within 5–10 % of the experimental value as determined from optical and resistivity measurements. We find that the experimental resistivity can be fit accurately to the standard Bloch-Grüneisen model with additional terms representing optical-mode coupling and electron-electron interactions. Previously used models did not conform to the correct Fermi-surface topology. Our *ab initio* results demonstrate that the transport properties of RuO_2 exhibit "normal" behavior as described by the Boltzmann equation.

I. INTRODUCTION

Ruthenium dioxide crystallizes in the rutile structure and exhibits metallic conductivities[1–7] comparable to the first half of the transition-metal series.[8] With its low resistance and high thermal stability, RuO_2 has been shown to be an excellent diffusion barrier between Al and Si in contact metallizations for use in very large scale integrated circuits,[9] as an electrical contact material,[10] strip-line conductor,[11] and for thin[12] and thick[13] film resistors in integrated circuits. While the high conductivity of RuO_2 lends itself to many applications in the microelectronics industry, a fundamental understanding of the intrinsic conduction mechanism has been lacking. Our *ab initio* calculations are intended to provide a better understanding of the transport properties of RuO_2, as well as other metalliclike transition-metal dioxides occurring in the rutile structure.[3]

A great deal of effort has gone towards understanding the electronic-transport properties of transition metals. These are now well understood in terms of the Fermi-liquid theory[14–19] for which a Boltzmann equation exists,[20] provided that the propagating quasiparticles are well defined and the electron mean-free-path length is of sufficient magnitude, i.e., $l \gg d$, where d is the interatomic spacing.[14,21] For the transition metals, it has been observed[15,17] that "normal" transport behavior exists for $l > 10$ Å. While considerable work has been performed to understand the anomalous transport properties in the high-temperature superconducting oxides,[14] very little has been performed on the "normal" transport behavior in transition-metal oxides.[21,22] Traditionally, transition-metal oxides have been one of the most difficult classes of solids to perform first-principles pseudopotential calculations owing to the localized nature of the transition-metal d and O $2p$ valence wave functions.[23] With the recent advances in techniques for generating soft-core transferable pseudopotentials,[24] and fast iterative diagonalization techniques,[25] we are now in a position to handle these complex systems from a first-principles approach.

The resistivity is defined as the inverse of the conductivity tensor[17,19]

$$\sigma_{\alpha\beta}=(\Omega_p^2\tau)_{\alpha\beta}/4\pi\ , \tag{1}$$

where $1/\tau_{\alpha\beta}$ and $\Omega^2_{p,\alpha\beta}$ are the tensorial components of the scattering rate and squared plasma frequency, respectively. The plasma-frequency tensor can be calculated from a knowledge of the electronic structure of the system and is given by

$$\Omega^2_{p,\alpha\beta}=-\frac{8\pi e^2}{V_{\text{cell}}}\sum_{n\mathbf{k}} v_{n\mathbf{k}_\alpha} v_{n\mathbf{k}_\beta}\frac{\partial f_{n\mathbf{k}}}{\partial \epsilon_{n\mathbf{k}}}\ , \tag{2}$$

where V_{cell} is the cell volume, $v_{n\mathbf{k}_\alpha}=\hbar^{-1}\partial\epsilon_n\mathbf{k}/\partial k_\alpha$ is the α component of the quasiparticle group velocity at $\mathbf{k}$ for the nth band, $\epsilon_{n\mathbf{k}}=E_{n\mathbf{k}}-E_F$ where E_F is the Fermi energy, and $f_{n\mathbf{k}}$ is the quasiparticle distribution function. A factor of 2 has been included to account for spin degeneracy. The scattering-rate tensor for electron transport resulting from electron-phonon scattering is given by[26]

$$\frac{\hbar}{\tau_{\mathrm{tr},\alpha\beta}}=4\pi k_B T\int_0^\infty \frac{d\omega}{\omega}\alpha^2_{\mathrm{tr},\alpha\beta}F(\omega)\left[\frac{\hbar\omega/2k_BT}{\sinh(\hbar\omega/2k_BT)}\right]^2, \tag{3}$$

where the spectral function $\alpha^2_{\mathrm{tr},\alpha\beta}F(\omega)$ is similar to that used in the Eliashberg theory of superconductivity.[14,27] The plasma-frequency tensor depends solely on the quasiparticle distribution, while the scattering-rate tensor depends upon the electron-phonon coupling. As the temperature of the conduction electrons is much greater than the average energy from other excitations such as phonons, we can replace the gradient of the quasiparticle distribution function by a delta function: $-\partial f_{n\mathbf{k}}/\partial\epsilon_{n\mathbf{k}}=\delta(\epsilon_{n\mathbf{k}})$. This represents the lowest-order approximation to the transport coefficients with respect to temperature. Although the temperature dependence of $\Omega_{p,\alpha\beta}$ has been explicitly removed, it implicitly remains through changes in the band structure resulting from temperature variations in the lattice constants. However, RuO_2 exhibits an anomalous dependence in the linear thermal-expansion coefficients for directions perpendicular, $\alpha_\perp$, and parallel, $\alpha_\parallel$, to the c axis. Experimental[28] results show that with increasing temperature, c decreases while a increases; the ratio $\alpha_\parallel/\alpha_\perp$ being approximately -0.3 throughout the temperature range of 20–1200 °C. However, it is not known *a priori* whether this anomaly will effect the plasma frequency and the resistivity through changes in the Fermi-surface topology.

Typically the scattering rate for many metals follows a Bloch-Grüneisen (BG) type behavior[29] which may be obtained by replacing $\alpha^2_{\mathrm{tr},\alpha\beta}F(\omega)$ with its Debye approximation:[21,27]

$$\alpha^2_{\mathrm{BG},\alpha\beta}F(\omega)=2\lambda_{\mathrm{BG},\alpha\beta}(\omega/\omega_D)^4\theta(\omega_D-\omega), \tag{4}$$

where θ is the Heaviside step function, ω_D is the Debye frequency, and λ_{BG} is the transport electron-phonon coupling constant in the BG model. Substituting the above expression into Eq. (3) and integrating results in the BG form of the electron-phonon scattering rate:

$$\frac{\hbar}{\tau^{\mathrm{BG}}_{\alpha\beta}}=8\pi k_B T\lambda_{\mathrm{BG},\alpha\beta}\left[\frac{T}{\Theta_D}\right]^4 J_5(\Theta_D/T), \tag{5}$$

where J_5 is a standard transport integral[29] defined by

$$J_n(\Theta_D/T)=\int_0^{\Theta_D/T}\frac{x^n dx}{4\sinh^2(x/2)}. \tag{6}$$

The BG form of the resistivity given above results in a temperature dependence[30] which is proportional to T^5 at low temperatures, and to T at high temperatures.

At low temperatures, the resistivity is dominated by impurities, vacancies, and various other defects. For low defect concentrations, these contributions are frequently assumed to be independent of temperature; the $T=0$ limit being defined as the residual resistivity ρ_0. The intrinsic resistivity, resulting from electron-electron and electron-phonon interactions, can be written as $\rho_i(T)=\rho(T)-\rho_0$. This is generally referred to as Matthiessen's rule,[29] and assumes that the various scattering mechanisms are uncorrelated or independent of one another; a condition typically not met in highly resistive materials.[31] Varying the defect concentration via different samples would result in a constant shift in the intrinsic resistivity for materials complying with Matthiessen's rule. The low-temperature resistivity is often used to assess sample purity for various growth conditions as in the case of RuO_2 where a majority of the experimental resistivity measurements have been performed.[4–6] For $T>\Theta_D$, the primary scattering mechanism arises from electron-phonon interband and intraband scattering. This mechanism is the major contribution to the high-temperature resistivity. The difficulty, however, in analyzing experimental results lies in the fact that many scattering mechanisms have the same temperature dependence. It becomes difficult to distinguish between two or more competing scattering events over a given temperature range. This is borne out in the present investigation, where we show that the standard model used to interpret the experimental resistivity of RuO_2 is virtually identical to a more conventional model based upon our electronic-structure calculations and Fermi-surface topology. The intrinsic scattering, whether electron-phonon or electron-electron induced, is largely determined by the Fermi-surface topology which governs the electron scattering. In the case of RuO_2, the Fermi surface has been experimentally probed by magneto-thermal oscillations,[32] magnetoresistance,[33] Azbel'-Kaner cyclotron resonance,[34] and de Haas–van Alphen measurements.[35] With the resistivity studies, Fermi-surface measurements, and band-structure calculations, we can assess the major scattering mechanisms to further understand normal transport in transition-metal oxides.

Owing to the tetragonal symmetry of the rutile structure, the conductivity tensor of Eq. (1) is diagonal in a principal-axis coordinate system. This results in a diagonal resistivity tensor, $\rho_{\alpha\alpha}=4\pi/(\Omega_p^2\tau)_{\alpha\alpha}$, with one component perpendicular, ρ_{xx}, and one parallel, ρ_{zz}, to the principal c axis. Considering the highly anisotropic nature of the RuO_2 lattice, i.e., $c/a\sim0.7$, one would expect that $\rho_{xx}>\rho_{zz}$ if conduction was to occur between Ru atoms, as the distance between neighboring Ru atoms is much smaller along the c axis. This is not what is found experimentally.[2] In Fig. 1, we show the single-crystal resistivity measurements[2] (solid circles) in the [001] and [100] directions, i.e., ρ_{zz} and ρ_{xx}. The residual resistivity from impurity scattering has been subtracted out assuming Matthiessen's rule to hold.[2] Since both components of the resistivity are shown in Fig. 1, it is evident, within the experimental error, that the electrical resistivity of RuO_2 is isotropic in the temperature range of 10–1000 K, i.e., $\rho_{zz}=\rho_{xx}$. This isotropy implies that $(\Omega_p^2\tau)_{zz}=(\Omega_p^2\tau)_{xx}$. Further, as the isotropy occurs over a rather broad temperature range, one expects $\Omega_{p,\alpha\alpha}$ and $\tau_{p,\alpha\alpha}$ to be approximately equivalent for the xx and zz components. This can be rationalized in terms of the typical Bloch-Grüneisen behavior, which describes the temperature-dependent electron-phonon scattering given by Eq. (5). Since $\Omega_{p,\alpha\beta}$ is only a weak function of temperature, one would expect any anisotropy in the scattering

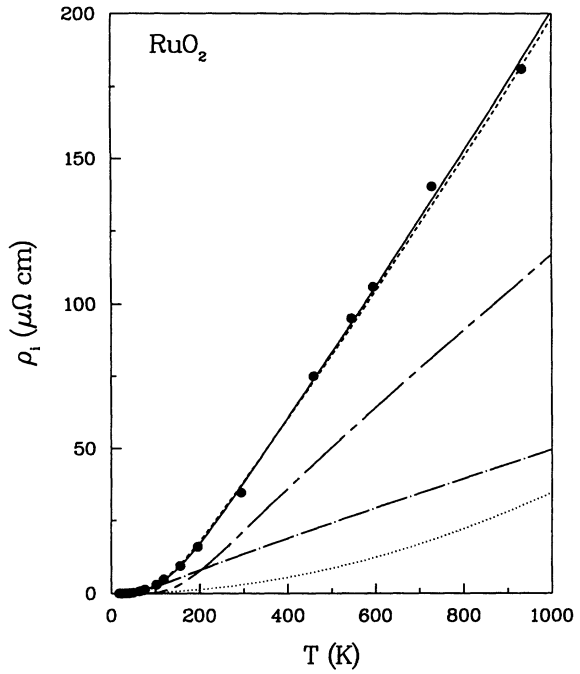

FIG. 1. Intrinsic electrical resistivity (Ref. 2), (●), in the [001] and [100] directions for RuO_2. The solid line represents the present model with a standard Bloch-Grüneisen (chain-dot) and an optical contribution (chain-dash) contribution for the electron-phonon interactions, and an electron-electron T^2 dependence (dotted). The dashed line represents a two-band model for the electron-phonon interactions typically used to fit to the experimental measurements along with a T^2 dependence for electron-electron interactions at low temperatures.

rate, given by $\lambda_{tr,xx}/\lambda_{tr,zz}$ for the tetragonal lattice, to be observable over this temperature range. Typically however, it is assumed that $\lambda_{tr,\alpha\beta}$ is only a weak function of crystal orientation,[21] where any anisotropy is usually accounted for by $\Omega_{p,\alpha\beta}$. In some cases however, the anisotropy in $\Omega_{p,\alpha\beta}$ is opposite to that of $\lambda_{tr,\alpha\beta}$ yielding approximately isotropic resistivities.[17]

For RuO_2, the intrinsic temperature dependence of the experimental[2] resistivity deviated from Matthiessen's rule, indicating that scattering rates between impurities, electrons, and phonons are not entirely independent from one another. However, as seen in Fig. 1, the deviation from Matthiessen's rule appears to be small considering that three RuO_2 samples are included in the experimental results.[2] It was further observed that the form of the resistivity differed significantly from the usual Bloch-Grüneisen behavior, but could be fit reasonably well to a two-band model.[36,37] This model describes the electron-phonon scattering in transition metals with parabolic s and d bands. An additional term proportional to T^2 was included to describe the low-temperature electron-electron scattering.[29] The electron-phonon interband scattering in this model is based on electrons being scattered from a Fermi sheet with high mobility and low band mass to one of low mobility and high band mass. The corresponding contribution to the resistivity is given by[2] $\rho_3 T^3[J_3(\Theta_D/T)-J_2(\Theta_G/T)]$, where ρ_3 is a constant, and $k_B\Theta_G$ is the minimum phonon energy needed to induce an intraband transition between the two Fermi sheets. At high temperatures, the same linear dependence in temperatures as the BG form is obtained, while at low temperatures the resistivity is proportional to T^3. In Fig. 1, we illustrate a fit (dashed line) to the experimental resistivity[2] using this model. As shown below however, the RuO_2 Fermi surface exhibits no such topology, which would indicate such a high degree of interband transitions between Fermi sheets. Previously experimental investigations have been based on this model, illustrating the difficulty in predicting scattering mechanisms based upon the goodness of fit. To stress this, we show in this figure a fit to the experimental data[2] with the typical Bloch-Grüneisen model given by Eq. (5) with an additional contribution to account for optical-mode coupling. This electron-phonon contribution can be obtained by substituting the Einstein approximation for $\alpha^2_{tr,\alpha\beta}F(\omega)$; this is given by

$$\alpha^2_{E,\alpha\beta}F(\omega)=\tfrac{1}{2}\omega_E\lambda_{E,\alpha\beta}\delta(\omega-\omega_E)\ , \tag{7}$$

which upon substituting into Eq. (3) yields

$$\frac{\hbar}{\tau^E_{\alpha\beta}}=2\pi k_B T\lambda_{E,\alpha\beta}\left[\frac{\Theta_E/2T}{\sinh(\Theta_E/2T)}\right]^2 . \tag{8}$$

We also have included in our model a term in the resistivity to account for electron-electron scattering[29] as in the case of previous models.[2] The resulting values of Θ_D and Θ_E were found to be 409 and 787 K, and the corresponding electron-phonon coupling constants $\hbar\Omega_p/\sqrt{\lambda_{BG}}$, and $\hbar\Omega_p/\sqrt{\lambda_E}$ were found to be 9.0 and 5.7 eV, respectively. As seen in this figure, both models fit the data reasonably well; however, the model presented here is in agreement with the Fermi-surface topology as shown below.

For transition-metal oxides, the inclusion of optical-mode coupling is a natural extension to the BG form of the resistivity, which only describes metals with a single-atom basis, i.e., acoustical-mode coupling. The addition of O leads to a large number of optical phonons; in the case of RuO_2 there are 15 possible optical modes which the electrons can scatter from. If the optical-mode frequencies are comparable to the experimentally observed frequency between scattering events, optical-mode coupling becomes a possible scattering mechanism. The value of the Einstein frequency, corresponding to the "dominant" optical mode, from our fit was found to be 547 cm^{-1}. While a detailed experimental or theoretical study of the optical-phonon modes in RuO_2 is lacking, zone-center Raman-active (RA) modes have been measured.[38] Of the four RA modes, the doubly degenerate E_g mode of 528 cm^{-1} is close to the Einstein frequency predicted from our model. At room temperature, the estimated frequency between scattering events (see Sec. III) was found to be 416 cm^{-1}, which is in the range at which optical-mode coupling can occur.

II. METHODS OF CALCULATION

The electronic-transport properties of RuO_2 were calculated within the local-density approximation employing the exchange-correlation potential of Ceperley and Alder.[39] Our *ab initio* total-energy calculations implemented a plane-wave basis in conjunction with soft-core pseudopotentials constructed by the method of Troullier and Martins[24] and transformed using the separation technique proposed by Kleinman and Bylander.[40] Plane waves up to an energy cutoff of 64 Ry were included in the calculation, while the structural and electronic properties were calculated with six **k** points generated by a Monkhorst-Pack[41] (3×3×3) grid with a shift vector of $(\frac{1}{2},\frac{1}{2},\frac{1}{2})$. We have used the Gaussian broadening scheme of Fu and Ho[42] to minimize the number of **k** points needed to sample the charge density. This scheme accounts for variations in the metal band occupancies near the Fermi level as a result of charge-transfer oscillations during the self-consistency cycle. We found that a Gaussian width of 10 mRy gave rapid convergence in the total energy. The above prescription resulted in total energies which were converged to within 0.05/atom. We have recently shown[23] that the above methodology gives good results for the static electronic and structural properties of RuO_2 and TiO_2.

Here we extend our previous study[23] by examining the electronic-transport properties of RuO_2. The structural parameters were determined by minimizing the total energy of the RuO_2 lattice. In Table I we compare our present *ab initio* results with the experimental room-temperature values of Boman.[43] Our theoretical results are within 2% of experiment as is typical of local-density calculations. The resulting band structure is shown in Fig. 2 along various high-symmetry directions of the irreducible Brillouin zone. Also shown in this figure is the corresponding electron density of states calculated by the linear tetrahedron method[44] using 726 **k** points. The Fermi energy has been taken as the reference energy and is indicated by the dashed line. A detailed comparison of the present band structure to previous experimental and theoretical results has been published elsewhere.[23]

The first 12 bands are predominantly O $2p$ in character while the O $2s$ manifold, not shown, is $\sim 18-19$ eV below E_F. The next ten bands are predominantly Ru $4d$ in character. These ten bands can be grouped into two distinct manifolds, which are reminiscent of the splitting of the Ru $4d$ states into a triply degenerate t_{2g} and doubly degenerate e_g states in the presence of an octahedral field of O^{2-} ions. In the rutile structure, the perfect O_h symmetry at the Ru site is lowered to D_{2h}, which subsequently causes the t_{2g} and e_g states to split into singly degenerate states. Since the compression of the octahedron along its principal axis[23] is only 2% in RuO_2, and since a clear distinction between these two manifolds exist, we have taken the O_h nomenclature for simplicity. The first six bands above the O $2p$ manifold are Ru t_{2g} derived while the next four are e_g derived. The last band shown is of Ru sp character.

TABLE I. Comparison of the experimentally determined structural parameters (Ref. 43) for RuO_2 in the rutile structure compared with the present *ab initio* results.

Property	Theory	Experiment
a (Å)	4.56	4.492
c (Å)	3.16	3.106
u	0.307	0.306

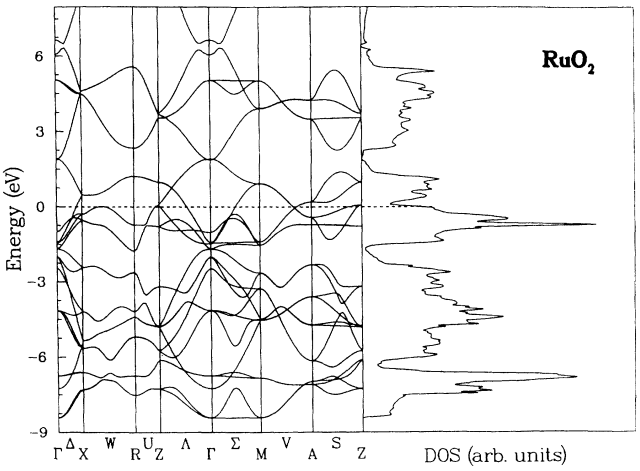

FIG. 2. Band structure for RuO_2 along high-symmetry directions of the irreducible Brillouin zone and the corresponding electron density of states. The energy zero has been taken as the Fermi energy.

In RuO_2, it is assumed that the t_{2g} manifold is divided into orbitals perpendicular, $t_\perp$, and parallel, $t_\parallel$, to the c axis. The $t_\parallel$ band is Ru-Ru derived with $d_{x^2-y^2}$ (a_g) orbital symmetry, while the $t_\perp$ is composed of Ru-O-derived π-bonding states with d_{yz} (b_{3g}) and d_{xz} (b_{2g}) orbital symmetry. The symmetry labels in parentheses are for the Ru atomic d states in a crystal field of orthorhombic, D_{2h}, symmetry. The $t_\parallel$ bands are typically assumed to be fully occupied, and therefore do not contribute to the RuO_2 conductivity, which results from the partially occupied $t_\perp$ bands. This is in agreement with the experimental observations. The anisotropic nature of the c/a ratio in RuO_2 would result in $\rho_{xx} > \rho_{zz}$ if conduction were to occur via the $t_\parallel$ bands as a result of a strong Ru-Ru overlap. However, as the Fermi level lies in the $t_\perp$ manifold, derived from Ru-O interactions, one would expect that $\rho_{xx} \approx \rho_{zz}$ owing to the approximate equivalence of the Ru-O equatorial and apical bond lengths, which differ by only 2%. The higher-lying, unoccupied e_g orbitals are comprised of Ru-O σ character with d_{xy} (b_{1g}) and d_{z^2} (a_g) orbital symmetry. In Figs. 3 and 4 we illustrate these orbitals in various planes of the tetragonal lattice, using the local Ru and O coordinate system of Munnix and Schmeits,[45] from the wave functions calculated at $\mathbf{k}_R = (\frac{1}{2},0,\frac{1}{2})$. These figures illustrate the localized nature of the O $2p$ and Ru $4d$ valence wave functions, which have previously caused difficulties when using traditional pseudopotentials. Although the charge residing on the O atoms in Fig. 3(c) is negligible, a significant amount of charge is observed in planes not shown. We point this

out as Figs. 3(a) and 3(c) could otherwise be interpreted as bonding and antibonding states resulting from a split in the Ru-Ru-derived bonding band. Such behavior would indicate a propensity for the RuO_2 lattice to transform to a distorted variant of the rutile structure. These transformations are commonly found in other transition-metal dioxides, e.g., VO_2, in which metal-atom pairing occurs along the c axis, causing a split of $t_{\|}$ into bonding and antibonding bands.[3]

III. ELECTRON-TRANSPORT PROPERTIES

Fermi-surface properties were calculated using the Fourier interpolation scheme proposed by Pickett, Krakauer, and Allen[46] to fit to $\epsilon_{n\mathbf{k}}$ using a grid of 726 **k** points in the irreducible Brillouin zone (BZ) and 1548 star functions in the expansion. The resulting Fermi surface was virtually identical to our previous results.[23] Specifically, the fifth t_{2g} band forms a spherically distort-

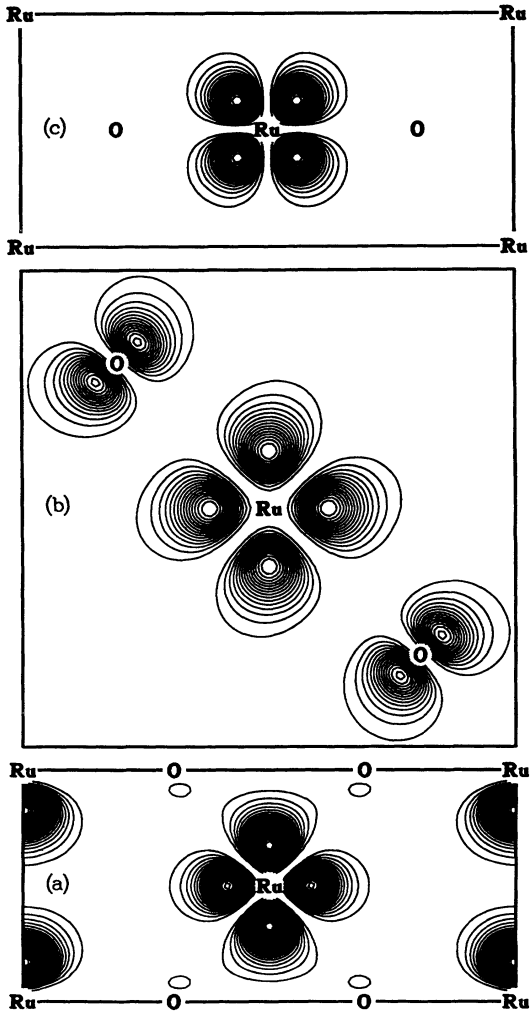

FIG. 3. Pseudocharge density contour plots of the t_{2g} (a) $d_{x^2-y^2}(a_g)$ in the (110) plane, (b) d_{xz} (b_{2g}) in the (002) plane, and (c) the d_{yz} (b_{3g}) orbital in the $(\bar{1}10)$ plane of the tetragonal RuO_2 lattice. Contours of constant charge density are separated by $1.5e/V_0$.

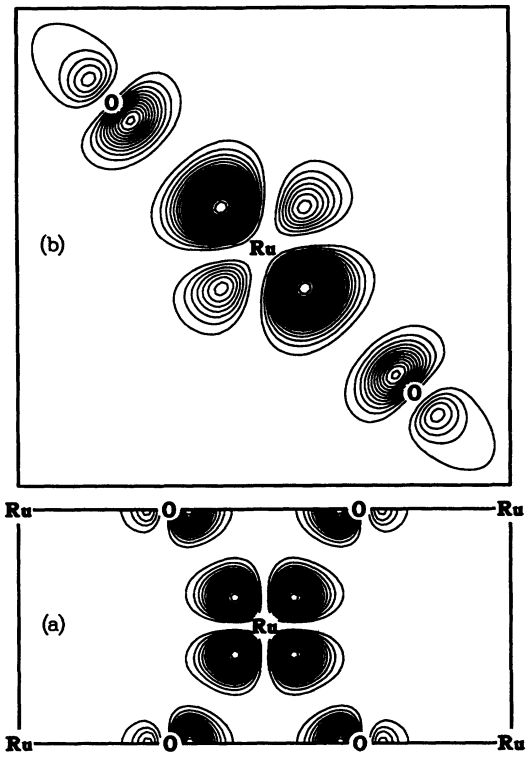

FIG. 4. Pseudocharge density contour plots of the e_g (a) d_{xy} (b_{1g}) in the (110) plane, and (b) the $d_{z^2}(a_g)$ orbital in the (002) plane of the tetragonal RuO_2 lattice. Contours of constant charge density are separated by $1.5e/V_0$.

ed electron sheet e_5 centered at Γ. The fourth t_{2g} band forms a hole sheet h_4 with arms in the $\{110\}$ planes. The third t_{2g} band forms a hole sheet h_3 centered at Z. While a detailed mapping of the Fermi surface for RuO_2 has not been previously performed, our results are in good agreement with the empirical model proposed by Graebner, Greiner, and Ryden[32] based on experimental magneto-thermal oscillations.

The plasma-frequency tensor, defined by Eq. (2), was transformed to a surface integral which was numerically evaluated using the linear tetrahedron method.[44] Band energies within the t_{2g} manifold were calculated from the Fourier interpolation scheme[46] using 2176 **k** points in the irreducible BZ. The corresponding values of $\Omega_{p,xx}$, and $\Omega_{p,zz}$ were found to be identical with a value of 3.3 eV. To test the convergence in $\Omega_{p,\alpha\alpha}$, calculations were performed with 726 **k** points. The corresponding values of $\Omega_{p,xx}$, and $\Omega_{p,zz}$ were found to be 3.3 and 3.2 eV, respectively. In Fig. 5, we illustrate the energy dependence of $\Omega_{p,xx}$, and $\Omega_{p,zz}$ in the vicinity of the Fermi energy. As seen in this figure, $\Omega_{p,xx}$, and $\Omega_{p,zz}$ track each other throughout the t_{2g} manifold with the perpendicular component on average being somewhat higher. The plasma-frequency components vary rapidly in the vicinity of the Fermi energy with $d\hbar\Omega/dE$ being approximately -6, resulting in an estimated accuracy of ± 0.1 eV for the plasma-frequency components.

Two characteristic features of a plasmon mode are

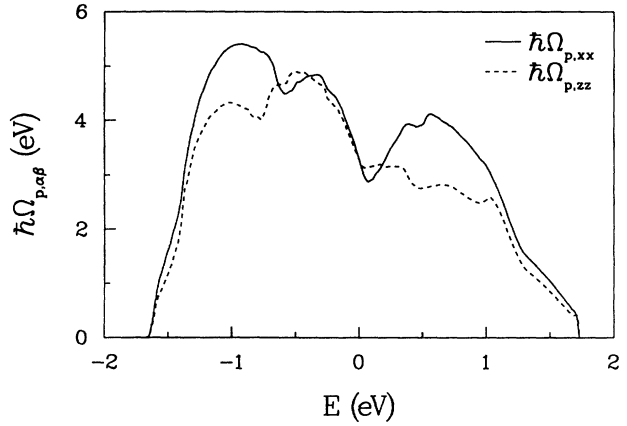

FIG. 5. Theoretical plasma energies for directions perpendicular, $\hbar\Omega_{p,xx}$ (solid), and parallel $\hbar\Omega_{p,zz}$ (dashed) to the c axis. The energy zero has been taken as the Fermi energy.

$\mathrm{Re}[\epsilon(\Omega_p)]=0$, where $\epsilon(\omega)$ is the complex dielectric function, and a pole or resonance in the energy-loss function at the plasma frequency. Electron energy-loss spectroscopy (EELS) often provides the most direct determination of the plasma energy for metals displaying free-electron-like behavior. The loss function can also be determined from reflectivity measurements and is proportional to $-\mathrm{Im}[1/\epsilon]$. Difficulties arise however, when interband transitions occur at energies lower than the plasma frequency. These interband transitions result in Drude-like plasma frequencies which are higher in energy than those that would be predicted by the roots of $\mathrm{Re}[\epsilon]$.

Examination of the experimental ϵ_1 curves for RuO_2 shows strong interband transitions with a threshold much lower than the plasma frequency. The fact that these interband contributions do not result in $\epsilon_1=0$ indicates that the transition are too low in energy to mediate a crossing effectively.[47] This is in fact shown by our present calculations where we find interband transitions down to 0.07 eV. In Fig. 6, we illustrate the energy-loss function, $-\mathrm{Im}[1/\epsilon]=\epsilon_2/(\epsilon_1^2+\epsilon_2^2)$, determined from the experimental[48] values of ϵ_1 and ϵ_2. The low-energy peaks

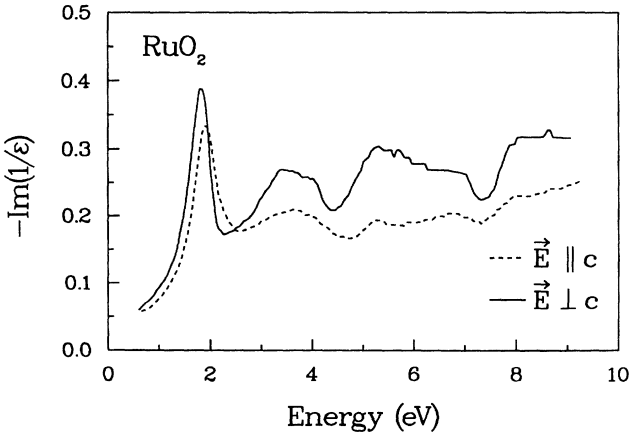

FIG. 6. Energy-loss function $-\mathrm{Im}[1/\epsilon]$ determined from experimental reflectivity measurements (Ref. 48).

occurring at 1.8 and 1.9 eV for the perpendicular and parallel components, respectively, are the experimental roots of ϵ_1. These peaks are interpreted as a result of interband transition, while the higher resonance peaks, occurring at approximately 3.7 eV, are interpreted as the plasma frequency. This value is in good agreement with our theoretical result of 3.3 eV.

Experimental electron energy-loss spectra[49] reveal a prominent loss feature at an energy of 1.78 eV. This feature was subsequently assigned to a surface plasmon feature of RuO_2. Although difficult to observe due to the experimental resolution, a higher-energy feature at approximately 3.4 eV is seen in the high-energy EELS spectra. This higher-energy feature is indicative of a bulk plasmon as the feature disappears on lowering the electron energy. The lower-energy feature we attribute to interband transitions rather than a surface mode. This type of behavior in which interband transitions dominate the EELS is common among other transition-metal oxides.[50] The above interpretation of the experimental EELS results in a plasma frequency which is in excellent agreement with our theoretical results.

One can also infer a value of the plasma frequency indirectly using the limiting behavior of the electrical resistivity at high temperatures. At high temperatures we have shown that the models predict a linear temperature dependence in the electrical resistivity. This type of behavior can be shown[51] to be model independent where the scattering rate, given by a high-temperature expansion of the lowest-order variational solution to the Bloch-Boltzmann equation, is given by

$$\frac{\hbar}{\tau}=2\pi\lambda_{\mathrm{tr}}k_B T(1-\hbar^2\langle\omega^2\rangle_{\mathrm{tr}}/12k_B^2T^2+\cdots), \qquad (9)$$

where $\langle\omega^2\rangle_{\mathrm{tr}}$ is a weighted mean-square phonon frequency. The above equation is valid for $T\geq\Theta_D$ and is accurate to within 1% of highly converged solution to the Bloch-Boltzmann integral equation.[15] At temperatures $T\geq\Theta_D/2$ the first term in Eq. (9) is sufficient for $\sim 10\%$ accuracy.[14] Given the isotropic nature of the $(\Omega_p^2\tau)_{\alpha\beta}$ tensor, we can write the resistivity for RuO_2 as $\rho=4\pi/\Omega_p^2\tau$. Including only the first term in Eq. (9), and taking the derivative of the resistivity allows us to estimate the plasma frequency from the relation

$$(\hbar\Omega_p)^2=8\pi^2\lambda_{\mathrm{tr}}\hbar k_B\left[\frac{d\rho}{dT}\right]^{-1}, \qquad (10)$$

which is equivalent to what one would obtain with the Bloch-Grüneisen form for the high-temperature resistivity. The experimental values[2,3,5-7] of $\hbar\Omega_p/\sqrt{\lambda_{\mathrm{tr}}}$ for single crystals using the above equation were found to be in the range of 4.3 to 4.9 eV. Although Ryden, Lawson, and Sartain[2] have indicated that RuO_2 deviates from Matthiessen's rule, the small spread in the $\hbar\Omega_p/\sqrt{\lambda_{\mathrm{tr}}}$ values from different investigations indicates that the deviation is not significant enough to affect the magnitude of Ω_p.

Allen and co-workers[15-17] have shown for many metals that the electron-phonon enhancement factor for transport, λ_{tr}, is very similar to the electron-phonon mass

enhancement for superconductivity, λ, and that determined from specific-heat measurements, λ_γ. Estimates of λ_{tr} are better approximated by λ as determined from superconductivity measurements than those predicted from heat-capacity measurements.[15–17] However, superconductivity has not been observed for RuO_2 down to a temperature of 4.2 K. The electron-phonon mass-enhancement factor may be calculated from the experimental electronic specific-heat coefficient, γ_{exp}, through the relation

$$\gamma_{exp}/\gamma_{theory}=1+\lambda_\gamma \tag{11}$$

where the theoretical value of γ_{theory} is determined from the Sommerfeld approximation: $\gamma_{theory}=\pi^2 k_B^2 D(E_F)/3$. Using our theoretical $D(E_F)$ value of 1.7 states eV^{-1} $cell^{-1}$ $spin^{-1}$ we find $\gamma_{theory}=3.98$ mJ mol^{-1} deg^{-1}. Using the experimental value[52] of 5.77 mJ mol^{-1} deg^{-1} for γ_{exp} yields an electron-phonon mass-enhancement factor of 0.45. Using this value for λ_{tr} in Eq. (10), we find an experimental plasma frequency in the range of 2.9 to 3.3 eV which is in good agreement with our theoretical value of 3.3 eV.

We have also determined the electron-phonon enhancement factors from our present model. Assuming Matthiessen's rule to be valid, the electron-phonon coupling constant will be the sum of both optical- and acoustical-mode contributions. Using the results from our fit to the experimental data,[2] we obtain an average $\hbar\Omega_p/\sqrt{\langle\lambda\rangle}$ value of 4.8 eV. The corresponding electron-phonon coupling constants were found to be 0.14 and 0.33 for λ_{BG} and λ_E, respectively, the total electron-phonon coupling contribution, $\langle\lambda\rangle=\lambda_{BG}+\lambda_E$, being 0.47. This value is in good agreement with the experimental λ_γ determined from heat-capacity measurements,[52] and provides a self-consistent check on the validity of our model. With the values of λ_{BG} and λ_E we can also estimate the superconducting temperature T_c from the modified McMillian equation.[53] Using a value of $\hbar\omega_{log}/k_B=600$ K, where $\hbar\omega_{log}/k_B=\exp[(\lambda_{BG}(\ln\hbar\omega_D/k_B-\frac{1}{4})+\lambda_E\ln\hbar\omega_E/k_B)/\lambda]$ for the present model, and a value of $\mu^*=0.1$, we estimate $T_c\sim 5$ K. While superconductivity has not been observed down to 4.2 K, it would be interesting to address this possibility at lower temperatures.

The validity of the Boltzmann equation in describing the electron-transport properties of RuO_2 can be determined from the mean-free-path length l. Using experimental results and our band-structure calculations, l may be calculated from the relation: $l=\langle v^2\rangle_F^{1/2}\tau_{tr}$ where $\langle v^2\rangle_F^{1/2}$ is the root-mean-squared velocity, averaged over the Fermi surface, and can be obtained from our plasma-frequency calculations where $\Omega_{p,\alpha\beta}^2=8\pi e^2 D(E_F)\langle v_\alpha v_\beta\rangle_F$ with $\langle v^2\rangle_F=2\langle v_x^2\rangle_F+\langle v_z^2\rangle_F$ for the tetragonal lattice. Using the values from our band-structure calculations results in a value of 0.28×10^6 m/s for $\langle v^2\rangle_F^{1/2}$. An average time between scattering events can be obtained from the experimental resistivity measurements where $\bar\tau=4\pi/\rho\bar\Omega_p^2$. Using the experimental[2] room-temperature resistivity 35.2 $\mu\Omega$ cm yields a $\bar\tau$ value of 1.3×10^{-14} s resulting in a value of 36 Å for l. This value is much greater than the Ru-O apical bond length of 1.94 Å and insures the existence of a Boltzmann equation in describing the electron transport in RuO_2.

IV. SUMMARY

We have calculated the electronic-transport properties for RuO_2 in the rutile structure using first-principles electronic-structure calculations performed within the local-density approximation. Our *ab initio* pseudopotential calculations employed a plane-wave basis in conjunction with a fast iterative diagonalization technique. The calculated plasma-frequency tensor is isotropic in agreement with optical and transport measurements. Our *ab initio* value for $\Omega_{p,xx}$ and $\Omega_{p,zz}$ of 3.3 eV is within 5–10 % of the experimental value determined from resistivity measurements. We find that the experimental resistivity can be fitted accurately to the standard Bloch-Grüneisen model with additional terms representing optical-mode coupling and electron-electron coupling. We have shown that the experimental resistivity can be described by the standard Bloch-Grüneisen model with an additional contribution resulting from optical-mode coupling. This model is shown to give identical results to a previous model which is based on an incorrect Fermi-surface topology. Our results show that the *ab initio* transport properties in RuO_2 are explainable in terms of "normal" transport behavior based upon a solution to the Boltzmann equation.

ACKNOWLEDGMENTS

We would like to thank P. B. Allen and W. W. Schulz for helpful discussions. This work was supported by the Division of Materials Research, Office of Basic Energy Sciences, U.S. Department of Energy, under Grant No. DE-FG02-89ER45391 and by the Minnesota Supercomputer Institute.

[1] H. Schäfer, G. Schneidereit, and W. Gerhardt, Z. Anorg. Chem. **319**, 327 (1963).
[2] W. D. Ryden, A. W. Lawson, and C. C. Sartain, Phys. Lett. **26A**, 209 (1968); Phys. Rev. B **1**, 1494 (1970).
[3] D. B. Rogers, R. D. Shannon, A. W. Sleight, and J. L. Gillson, Inorg. Chem. **8**, 841 (1969).
[4] S. R. Butler and J. L. Gillson, Mater. Res. Bull. **6**, 81 (1971).
[5] M. W. Shafer, R. A. Figat, B. Olson, S. J. LaPlaca, and J. Angello, J. Electrochem. Soc. **126**, 1265 (1979).
[6] Y. S. Huang, H. L. Park, and F. H. Pollak, Mater. Res. Bull. **17**, 1305 (1982).
[7] P. Triggs, Helv. Phys. Acta **58**, 657 (1985).
[8] C. Kittel, *Introduction to Solid State Physics*, 6th ed. (Wiley, New York, 1986).
[9] E. Kolawa, F. C. T. So, E. T-S. Pan, and M-A. Nicolet, Appl. Phys. Lett. **50**, 854 (1987); L. Krusin-Elbaum, M. Wittmer,

and D. S. Ye, *ibid.* **50**, 1879 (1979).
[10]D. J. Pedder, Electrocompon. Sci. Technol. **2**, 259 (1976).
[11]M. W. Shafer and J. Armstrong, IBM Tech. Disc. Bull. **20**, 4633 (1978).
[12]Q. X. Jia, Z. Q. Shi, K. L. Jiao, W. A. Anderson, and F. M. Collins, Thin Solid Films **196**, 29 (1991).
[13]N. C. Halder, Electrocompon. Sci. Technol. **11**, 21 (1983); K. Bobran, and A. Kusy, J. Phys. Condens. Matter **3**, 7015 (1991).
[14]P. B. Allen, Comments Condens. Matter Phys. **15**, 327 (1992).
[15]P. B. Allen, T. P. Beaulac, F. S. Khan, W. H. Butler, F. J. Pinski, and J. C. Swihart, Phys. Rev. B **34**, 4331 (1986).
[16]P. B. Allen, Phys. Rev. B **36**, 2920 (1987).
[17]B. A. Sanborn, P. B. Allen, and D. A. Papaconstantopoulos, Phys. Rev. B **40**, 6037 (1989).
[18]W. W. Schulz, P. B. Allen, and N. Trivedi, Phys. Rev. B **45**, 10 886 (1992).
[19]P. B. Allen, W. E. Pickett, and H. Krakauer, Phys. Rev. B **37**, 7482 (1988).
[20]T. D. Holstein, Ann. Phys. (N.Y.) **29**, 410 (1964); R. E. Prange and L. P. Kadanoff, Phys. Rev. **134**, A 566 (1964).
[21]P. B. Allen and W. W. Schulz, Phys. Rev. B **47**, 14 434 (1993).
[22]W. W. Schultz, L. Forro, C. Kendziora, R. Wentzcovitch, D. Mandrus, L. Mihaly, and P. B. Allen, Phys. Rev. B **46**, 14 001 (1992).
[23]K. M. Glassford and J. R. Chelikowsky, Phys. Rev. B **47**, 1732 (1992); **46**, 1284 (1992).
[24]N. Troullier and J. L. Martins, Phys. Rev. B **43**, 1993 (1991).
[25]J. L. Martins and M. L. Cohen, Phys. Rev. B **37**, 6134 (1988); J. L. Martins, N. Troullier, and S.-H Wei, *ibid.* **43**, 2213 (1990).
[26]P. B. Allen, Phys. Rev. B **3**, 305 (1971).
[27]P. B. Allen, Phys. Rev. B **17**, 3725 (1978).
[28]K. V. K. Rao and L. Iyengar, Acta Crystallogr. Sect. A **25**, 302 (1969); G. Bayer, H. G. Wiedemann, Thermochim. Acta, **11**, 79 (1975).
[29]J. M. Ziman, *Electrons and Phonons,* 2nd ed. (Oxford University, Oxford, 1979).
[30]The function $J_n(x)$ has the following low- and high-temperature limits: $\lim_{T\to 0} J_n(\Theta_D/T)=n!\zeta(n)$, and $\lim_{T\to\infty} J_n(\Theta_D/T)=(\Theta_D/T)^{n-1}/(n-1)$.
[31]P. L. Rossiter, *The Electrical Resistivity of Metals and Alloys* (Cambridge University Press, Cambridge, 1991).
[32]J. E. Graebner, E. S. Greiner, and W. D. Ryden, Phys. Rev. B **13**, 2426 (1976).
[33]S. M. Marcus, Phys. Lett. **28A**, 191 (1968).
[34]R. T. Slivka and D. N. Langenberg, Phys. Lett. **28A**, 169 (1968).
[35]S. M. Marcus and S. R. Butler, Phys. Lett. **26A**, 518 (1968).
[36]N. F. Mott, Proc. Phys. Soc. London **47**, 571 (1935).
[37]A. H. Wilson, Proc. R. Soc. London, Ser. A **167**, 580 (1938).
[38]Y. S. Huang and F. H. Pollak, Solid State Commun. **43**, 921 (1982).
[39]D. M. Ceperley and B. J. Alder, Phys. Rev. Lett. **45**, 566 (1980); J. P. Perdew and A. Zunger, Phys. Rev. B **23**, 5048 (1981).
[40]L. Kleinman and D. M. Bylander, Phys. Rev. Lett. **48**, 1425 (1982).
[41]H. J. Monkhorst and J. D. Pack, Phys. Rev. B **13**, 5188 (1976).
[42]C.-L. Fu and K.-M. Ho, Phys. Rev. B **28**, 5480 (1983).
[43]C.-E. Boman, Acta Chem. Scand. **24**, 116 (1970).
[44]A. H. MacDonald, S. H. Vosko, and P. T. Coleridge, J. Phys. C **12**, 2991 (1979).
[45]S. Munnix and M. Schmeits, Phys. Rev. B **30**, 2202 (1984).
[46]W. E. Pickett, H. Krakauer, and P. B. Allen, Phys. Rev. B **38**, 2721 (1988); our values of c_1 and c_2 were taken as 0.25.
[47]R. F. Egerton, *Electron Energy-loss Spectroscopy in the Electron Microscope* (Plenum, New York, 1986), p. 164.
[48]A. K. Goel, G. Skorinko, and F. H. Pollak, Phys. Rev. B **24**, 7342 (1981).
[49]P. A. Cox, J. B. Goodenough, P. J. Tavener, D. Telles, and R. G. Egdell, J. Solid State Chem. **62**, 360 (1986).
[50]J. P. Kemp, S. T. P. Davies, and P. A. Cox, J. Phys. Condens. Matter **1**, 5313 (1989).
[51]B. Chakraborty, W. E. Pickett, and P. B. Allen, Phys. Rev. B **14**, 3227 (1976).
[52]B. C. Passenheim and D. C. McCollum, J. Chem Phys. **51**, 320 (1969).
[53]P. B. Allen and R. C. Dynes, Phys. Rev. B **12**, 905 (1975).